Proceedings of JRCICE2007
2007 ASME/IEEE Joint Rail Conference & Internal Combustion Engine Spring Technical Conference
March 13-16, 2007, Pueblo, Colorado, USA

JRC/ICE2007-40068

FLOW AND ATOMIZATION MODELS FOR C.R. DIESEL ENGINE CFD SIMULATION

Maria Cristina Cameretti **Raffaele Tuccillo**

Dipartimento di Ingegneria Meccanica per l'Energetica (D.I.M.E.), Università di Napoli Federico II (Italy)

ABSTRACT

In the present work, the authors investigate the spray evolution and, in particular, the atomization process in a diesel engine bowl by using the *KIVA3-V* computational code with different break-up models.

After a preliminary test of the break-up models sensitivity to the grid size and topology, the same atomization models are employed for the two-phase flow calculation in the combustion chamber of a common rail, turbocharged diesel engine conceived for future HCCI applications. The computations are extended to the combustion process in order to proceed with an overall validation with experimental engine test data characterized by variable EGR rates.

The liquid spray-air interaction is studied within a flow field generated by the previous gas exchange process, the external ducts being included in the computational domain. This allows a more realistic evaluation of the fuel-air mixing under the actual conditions occurring at different engine regimes.

NOMENCLATURE

B_1	constant in the Wave and KHRT model
CF1	pre-exponential factor in the kinetic equation
C_{RT}	constant in the KHRT model
r	droplet radius
T	Taylor number
u	relative velocity
We	Weber number
z	Cylinder axis direction
Z	Ohnesorge number

Greeks

μ_l	viscosity
ρ_g	gas density
ρ_l	liquid density
σ	superficial tension
τ	break-up time

INTRODUCTION

Most of engine manufacturers are interested in improving high pressure diesel injection (HPDI) systems as the most efficient way to meet the stringent emission targets of diesel engines. Although HPDI has nowadays become a standard, a continuous study of both the spray evolution and its interaction with air is essential to understand and improve the diesel combustion processes. A comprehensive overview of the spray structure, the break-up of the liquid fuel into droplets and the interaction between droplets and the turbulent gas flow field and coalescence as well [1-4], enhances the knowledge of the role of such physical processes for a more efficient combustion and a reduced quantity of exhaust pollution. More and more studies are currently carried out as to investigate the effects of changes in the operating conditions of the diesel injection system in terms of spray evolution and distribution in a combustion chamber of light duty, common-rail equipped diesel engines [4][6-10][13-15][17], [24].

Actually, a reliable prediction of the early phases that lead to the reactant ignition plays a fundamental role for a correct prediction of the combustion development. Basing on this assumption, the authors investigate in this paper the spray evolution and, in particular, the atomization process by using a 3-D computational code, the widely diffused KIVA3-V [5], with the comparison of different break-up models implemented. As shown in the following, the assessment of this task is of key importance, regardless of the combustion model employed, for proceeding with a reliable prediction of the whole in-cylinder process. Therefore, some spray computations are preliminarily performed in a diesel engine combustion chamber without swirled or tumbled flows, in order to test the break-up model sensitivity to the grid topology.

Then, the same atomization models are experienced in a common rail, turbocharged diesel engine chamber conceived for future extension to *HCCI* applications. Such computations

take into account the flow fields that take place after the gas exchange period. The engine simulation include the combustion process in order to achieve an overall validation with experimental engine test data, the latter referring to operation with increasing *EGR* rates [25]. Actually, the adoption of relevant levels of the exhaust recirculation aims at producing a smoother, low NOx emission combustion profile [23]. In this sense, such a process exhibits significant analogies with the one occurring in a continuous flow combustion chamber when approaching the Mild-Combustion regime, whose study the authors are currently carrying out [18, 19]. The main aspects of such a similitude consist of the high temperature of the reactant mixture and of the strong dilution with inert species, together with the fairly reduced temperature peaks throughout the chamber. The more updated *HCCI* [16, 20, 21, 22] engines can be therefore intended as a definite refinement of this concept.

This paper pays particular attention to the estimation of the combined effect of the EGR ratio and the injection timing for producing the desired smooth combustion profile. To this purpose the evaluation of actual conditions for the reactant mixture formation is worthy of particular care. Therefore, the liquid spray-air interaction is studied within a flow field generated by the previous gas exchange process, the external ducts being included in the computational domain. This allows a more realistic evaluation of the fuel-air mixing under the actual conditions occurring at different rates of exhaust recirculation.

THE ATOMIZATION MODELS

In the following, the atomization models that have been examined for the selection of the most appropriate one are briefly recalled.

The TAB model. The model is based on the TAB method [1] proposed by O'Rourke and Amsden which presents Taylor's analogy and considers the oscillating and distorting droplet and a spring-mass system:

$$m\ddot{x} = F - kx - d\dot{x} \tag{1}$$

The external force acting on the mass, the restoring force of spring, and the damping force are analogous to the gas aerodynamic force, the liquid surface tension force, and the liquid viscosity force, respectively:

$$\frac{F}{m} = C_F \frac{\rho_g u^2}{\rho_l r} \quad ; \quad \frac{k}{m} = C_k \frac{\sigma}{\rho_l r^3} \quad ; \quad \frac{d}{m} = C_d \frac{\mu_l}{\rho_l r^2} \tag{2}$$

$$\ddot{y} = \frac{C_F}{C_b}\frac{\rho_g}{\rho_l}\frac{u^2}{r^2} - \frac{C_k \sigma}{\rho_l r^3} y - \frac{C_d \mu_l}{\rho_l r^2}\dot{y} \quad ; \quad \frac{1}{t_d} = \frac{C_d}{2}\frac{\mu_l}{\rho_l r^2}$$

$$y(t) = \frac{C_F}{C_k C_b} We + e^{-t/t_d}\left[\left(y_0 - \frac{C_F}{C_k C_b} We\right)\cos\omega t + \frac{1}{\omega}\left(\dot{y}_0 + \frac{y_0 - \frac{C_F}{C_k C_b} We}{t_d}\right)\sin\omega t\right] \tag{3}$$

The dimensionless constants C_F, C_k, C_d are determined by comparing with one experimental and two theoretical results.

In shock tube experiments the critical Weber number for break-up was found to be $We_c \cong 6$. In these experiments $t_d \cong \infty$ and $y_0 = \dot{y}_0 = 0$. Thus from eq.(3):

$$y(t) = \frac{C_F}{C_k C_b} We(1 - \cos\omega t) \tag{4}$$

The model predicts break-up if and only if y>1, which occurs if and only if:

$$2\frac{C_F}{C_k C_b} We > 1 \tag{5}$$

Therefore the model gives the experimental result if:

$$\frac{C_k C_b}{C_F} = 2We_{crit} = 12 \tag{6}$$

The constant C_k is obtained by matching with the fundamental oscillation frequency: $C_k = 8$

For oscillations of the fundamental mode Lamb gives a value of $C_d = 5$ for the damping coefficient.

The Wave model. The Wave model [2] is based on the instability of the surface waves driven by the aerodynamic forces acting on the jet. The liquid jet, injected from the nozzle in the shape of blobs with a radius 'a' is broken into smaller droplets of radius 'r':

$$r = B_0 \Lambda \tag{7}$$

The law of variation of the blob radius 'a' due to break-up is:

$$\frac{da}{dt} = -(a - r)/\tau \tag{8}$$

The break-up time is expressed by:

$$\tau = \frac{3.726 B_1 a}{\Lambda \Omega} \tag{9}$$

where Λ is the wavelength of the most unstable wave disturbance and Ω is the maximum wave growth rate:

$$\Lambda = 9.02 r_0 \frac{(1+0.45Z^{0.5})(1+0.4T^{0.7})}{(1+0.87We_2^{1.67})^{0.6}}$$
$$\Omega = \frac{(0.34+0.38We_2^{1.5})}{(1+Z)(1+1.4T^{0.6})}\sqrt{\frac{\sigma}{(\rho_1 r_0^3)}} \tag{10}$$

We_2 being the Weber number: $We_2 = \dfrac{\rho_g u_r^2 r_0}{\sigma}$

Z the Ohnesorge number: $Z = \dfrac{\sqrt{We_1}}{\mathrm{Re}_1}$

T the Taylor number: $T = Z*We_2^{0.5}$

The two model constants B_0 and B_1 must be adjusted for a better fitting of the numerical results with the experimental ones. In particular, B_0 is set at the same value i.e., B_0 =0.61 by Reitz [3], Liu et al. [11] and Kong et al. [12] while in these works different values of B_1 in the range from 1.7 to 30 were chosen such as Belardini et al. [7] who carried out a sensitivity analysis of Wave model by varying the model break-up time constant.

The *KHRT* model The Kelvin-Helmholtz wave model and the Rayleigh-Taylor model have been implemented in *KIVA 3V* code [4]. The *KH* model is based on the Wave model [3] presented in the code and is used to predict the initial break-up of the injected blobs or the intact liquid core.

The Rayleigh-Taylor (*RT*) model is used in conjunction with the *KH* model to describe the secondary break-up of the droplets. This model predicts instabilities on the surface of the droplet that grows until a given characteristic break-up time when it breaks up. The droplet acceleration is:

$$a = \frac{3}{8} C_D \frac{\rho_g u_r^2}{\rho_l r} \tag{11}$$

where C_D is calculated as:

$$C_D = C_{D,sfera}\,(1 + 2.632y)$$

$$\Lambda_{RT} = 2\pi C_{RT}/K_{RT} \tag{12}$$

$$\Omega_{RT} = \sqrt{\frac{2}{3\sqrt{3\sigma}} \frac{|\, g_t(\rho_l - \rho_g)\,|^{3/2}}{\rho_l + \rho_g}}$$

where C_{RT} is an adjustable constant and K_{RT} is the wave number equal to: $\sqrt{\frac{|\, g_t(\rho_l - \rho_g)\,|}{3\sigma}}$

Once the *RT* waves have been growing for a time greater than the break-up time ($\tau_{RT} = C_\tau/K_{RT}$, where C_τ arbitrary constant equal to 1 usually), the droplet break-up happens. The new droplet radius is:

$$r_c = \pi C_{RT}/K_{RT} \tag{13}$$

CALCULATIONS AND RESULTS

In this study the computational results were obtained by using the KIVA-3v code [5] and they are referred to a set of experimental data of a four stroke, common-rail, turbocharged four-cylinder diesel engine with external EGR (table 1). Both the experiments and the numerical simulation were carried out to the aim of defining conditions for a smooth combustion development. In this sense, such activities can be intended as preliminary studies of the real HCCI operation.

The figure 1 represents the full computational domain that includes the inlet and exhaust ducts and valves. The cylinder and duct structured mesh was obtained by using the *ICEM* meshing tool.

Bore	84 mm
Stroke	90 mm
Connecting rod	136 mm
Volume Displacement	499 cm^3
Compression ratio	16

Table 1. Cylinder Data

Grid sensitivity and choice of the atomization model. Two types of grid sensitivity analysis were necessary for this computational case. The first one refers, as usual, to the grid size independence that was reached after with a mesh of 104000 cells (the cylinder and bowl volume discretizations being of nearly 58000 and 5000 cells, respectively). In addition, issuing a conformal structured mesh within a rather complex domain involves an unusual cell distribution within both cylinder and bowl regions (fig. 1), so that the behaviour of the several atomization models should be carefully checked.

Therefore, the final validation of the computational grid has been performed by varying both the mesh topology and the break-up models. In particular, for the atomization of the injected spray the TAB, *Wave* and *KHRT* models are used to analyse the grid sensitivity on spray predictions. In figure 2 the six jets are represented in the same operating conditions with the *TAB* model but with two different grid topologies, say the polar and cartesian ones. The symmetry of the jets is well simulated only with a polar grid and a higher penetration is observed too.

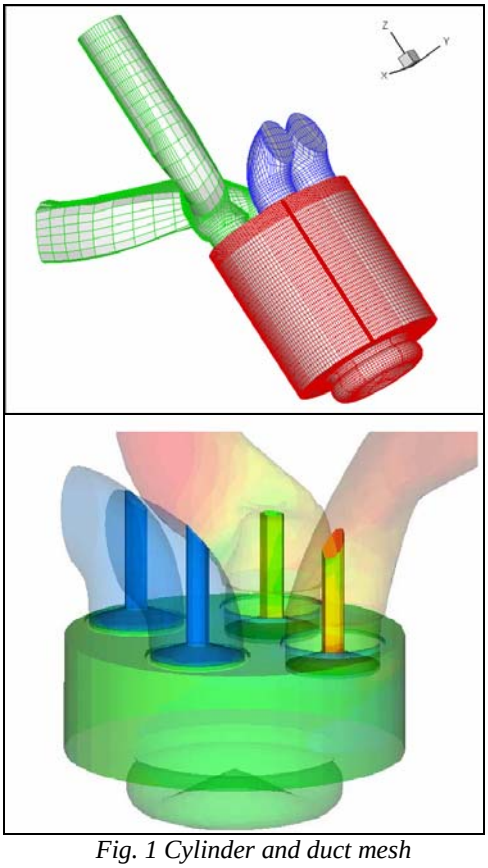

Fig. 1 Cylinder and duct mesh and computational domain

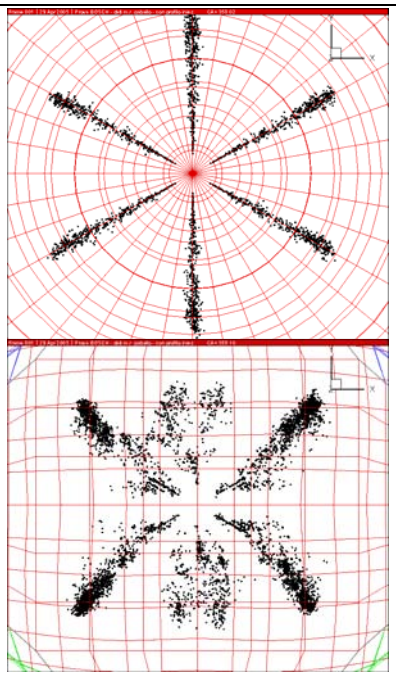

Fig. 2. Fuel jets in two different grids obtained with the TAB model.

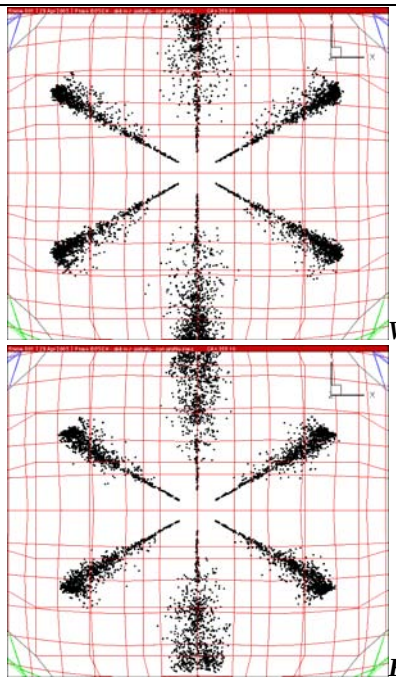

Fig. 3 .Fuel jets in a cartesian grid obtained with Wave and KHRT break-up models.

In figure 3, the droplet distribution is shown for the other two atomization models, *Wave* and *KHRT*, in a cartesian grid where the jet symmetry is fulfilled. In these last two cases the increased jet penetration lengths due to larger droplets overcomes the grid shape. The particular, tip penetration trend of two jets confirms the higher sensitivity of the TAB model to the grid: in fact, each jet presents a different penetration (fig.4).

Therefore, in this study the choice of the *Wave* model seemed to be the most appropriate for proceeding with the calculation of different engine operating conditions, by using the structured cartesian grid that results from the mesh generation consistent with the valve geometry. Once reached a satisfactory agreement with the experimental data, a final refinement with the *KHRT* model was experienced.

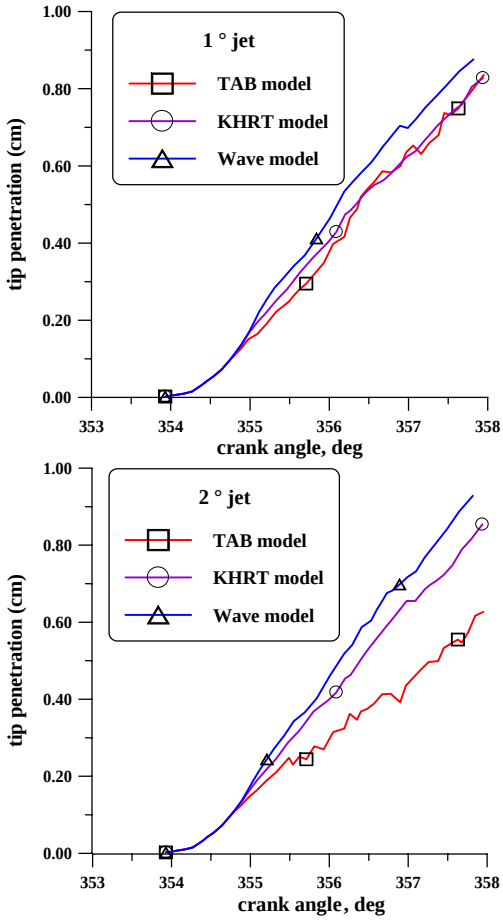

Fig. 4. Tip penetration of the first and the second jet with different break-up models.

Speed	*2000 rpm*		
Boost Pressure	*1.75 bar*		
Injected Fuel Mass	*2.2 *10^{-2} g/cycle*		
Oxidant / Fuel Ratio	*36.4*		
Rail injection pressure range	*1450 – 1650 bar*		
Nozzle	*6 holes*		
Hole diameter	*0.160 mm*		
EGR ratio	***0***	***27%***	***57%***
Fuel/Oxygen Equivalence Ratio	*0.432*	*0.453*	*0.528*
Fuel injection start (deg. ATDC)	*4.7*	*2.92*	*-5.3*
Fuel Injection Interval	*9.3 deg.*		

Table 2. Engine operating conditions

Simulation of engine operating conditions. The computational cases refer to a part-load condition (66% of full load, *BMEP* = 8bar), for three different EGR levels, according to the specifications given in table 2. The fuel injection timing

was determined in order to produce, in all cases, the auto-ignition at the approximately the same crank-angle. Therefore, the fuel injection is advanced as the EGR ratio increases, since the larger injection advance is compensated by higher ignition delays. The velocity profile of fuel injected is practically the same in all cases (fig. 5).

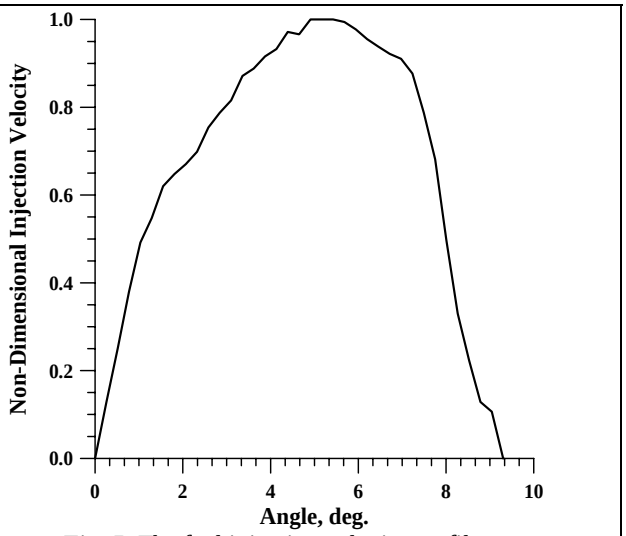

Fig. 5. The fuel injection velocity profile.

The choice for injection timing results in a relevant shift of the experimental pressure peak after the top dead center (fig. 6) and, mainly, in a smoother combustion profile than those usually induced by more advanced fuel injections, as shown in the following.

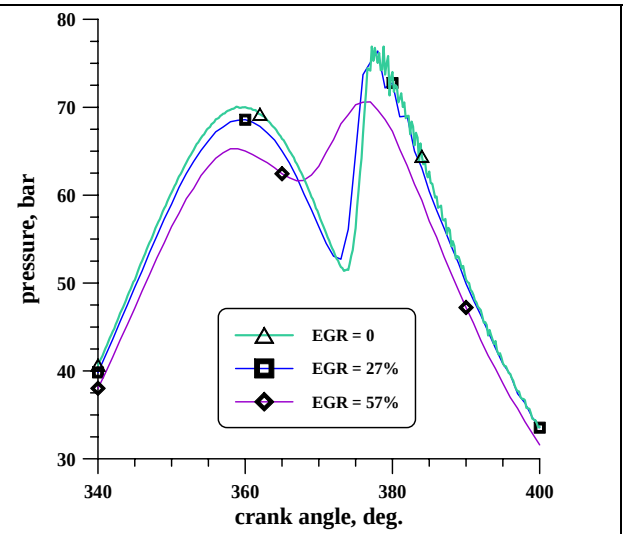

Fig. 6. Experimental in-cylinder pressure for different EGR levels.

The figures 7 and 8 show the computed in-cylinder average temperatures and the mass variation during the gas exchange for the three different EGR levels. The latter exhibit a practically identical behaviour, since the pressure at the inlet and exhaust duct boundaries are nearly the same for all cases. Regarding to the mean temperature profiles in fig. 7, these confirm that the combustion process attains a fairly lean development because of the combined effect of the injection timing and of the air dilution with the exhaust at the higher EGR rates.

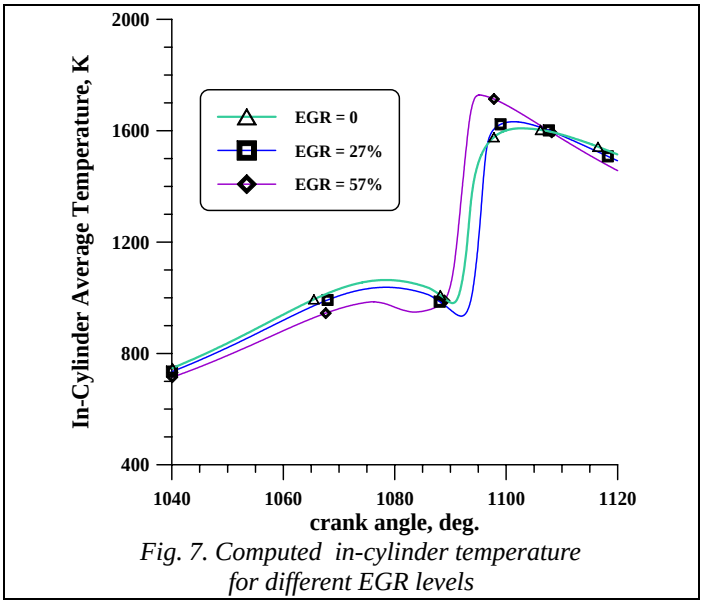

Fig. 7. Computed in-cylinder temperature for different EGR levels

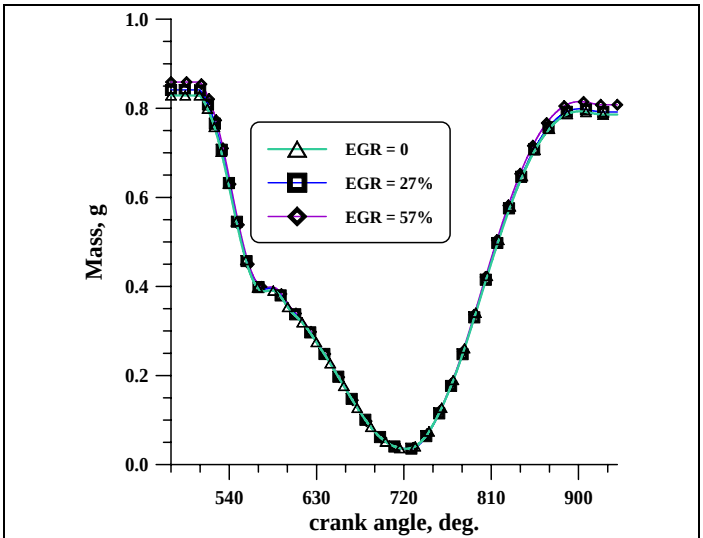

Fig. 8 In-cylinder mass variation during the gas exchange process for different EGR levels

Since the calculations include the open valve periods, more engine cycles are to be computed to reach the numerical convergence (fig. 9). The latter must be intended, for unsteady-periodical flow cases, as the achievement of a satisfactory periodicity of both the in-cylinder conditions and the external flow fields. In particular, at the third cycle the calculation is stopped since such a periodicity has been reached. The converged periodical results should ensure that the instantaneous local values of all the flow and thermo-chemical parameters only depend on the boundary conditions, regardless of the initial conditions assigned. The unsteady flow, open boundary, calculation include the two-equation, k-ε, turbulence model. Therefore the inlet boundary conditions consist of the

total pressure and temperature together with the turbulent kinetic energy and length scale. The inflow gas composition is assigned accordingly with the EGR level.

The attention being focused on the influence of both the flow conditions and atomization models, the combustion model employed for a full engine cycle calculation consists of the classical one-step kinetic mechanism of fuel oxidation within a finite rate – eddy dissipation approach [26]. The self-ignition is governed by the Stringer relationships [27] for the ignition delay. The latter are only sensitive to the local thermodynamic conditions and fuel/air ratio, so that the combustion simulation at the highest EGR levels would be worthy of a more refined modelling, by taking into account the relevant oxygen defect and the inert species contents. An attempt in this sense will be shown in the following, when referring to the 57% EGR case. The combustion simulation is completed by the system of chemical kinetic equations for the mechanism of thermal nitric oxide formation [28].

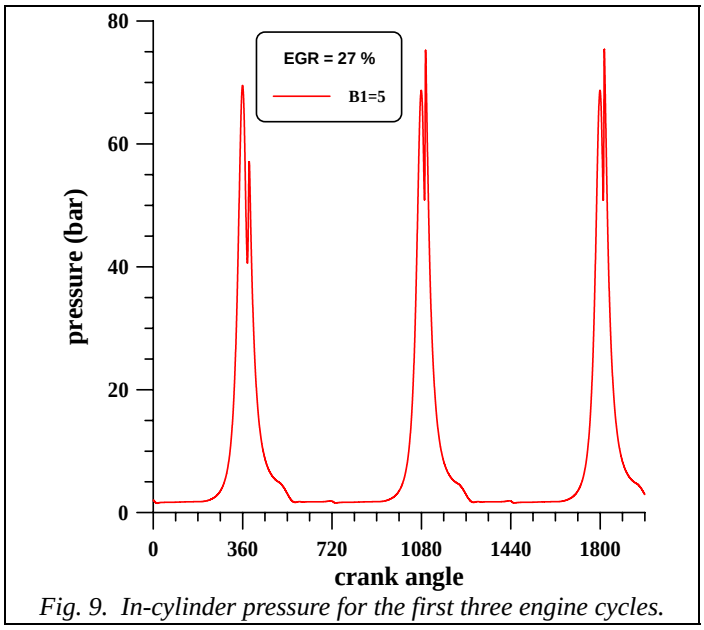

Fig. 9. In-cylinder pressure for the first three engine cycles.

For the baseline case (i.e., *EGR rate=0*) the effect of the *Wave* model B_1 constant on the in-cylinder pressure has been analyzed. As shown in figure 10, the best B_1 constant value to match experimental data is in the (5 – 7) range, although the ignition start is clearly advanced. The same values have been used in the case 2 (*EGR rate=27%)* as reported in figure 11 and case 3 (*EGR rate=57%*). For case 2 the B_1 constant is optimized to a value 5 for a better fitting of the experimental pressure curve. The same value was used in the third case (*EGR =57%*) but the longer ignition delay, due to the very high exhaust gas presence in cylinder, makes difficult the matching of numerical and experimental data. As expected, the only atomization model refinements are not sufficient, with the conventional models for ignition delay and fuel oxidation, to reproduce the actual combustion behaviour. To this aim, a *two-step* oxidation mechanism has been introduced to separate the CO from the CO_2 formation, like anticipated. In figure 12 the pressure trends are reported and compared to the *one-step* mechanism results, by varying the pre-exponential factor (*CF1*) of the first oxidation reaction respect to the standard value of $6x10^{+11}$. Some significant benefits can be detected when adopting the two-step approach with a lower *CF1*value. In this case a better reproduction of the early partial oxidation is obtained, as demonstrated by the satisfactory fitting of the slope of experimental pressure with the computational one.

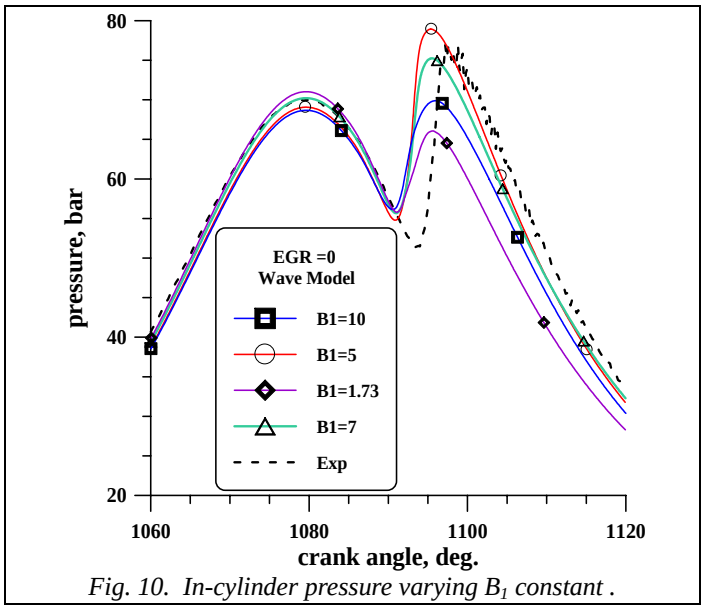

Fig. 10. In-cylinder pressure varying B_1 constant .

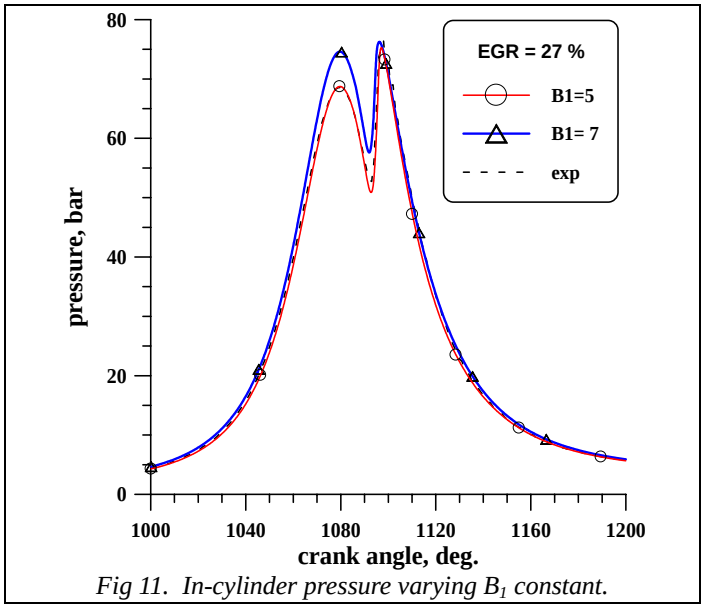

Fig 11. In-cylinder pressure varying B_1 constant.

In figure 13 the fuel burning rates are plotted for the three cases examined: a fairly smoother trend is obtained in the third case (EGR=57%) where the poor oxygen amount slows down the heat release rate. The introduction of the two-step mechanism confirms a more realistic prediction of the early combustion development which was already detectable in the experimental pressure curve in fig. 12.

Referring to the EGR = 27% case, in figures 14, 15, 16 the distribution of the swirl index (say, the ratio of the air *z-vorticity* to the engine angular speed) in both ducts and cylinder are displayed during the air inlet phase and at two

different positions along the compression stroke (80° BTDC and 20° BTDC respectively). These figures put properly into evidence that the air vorticity originates from the intake process and it partially extinguishes during the next phases. However, the swirl index still remains at a significant level when the piston is close to the top dead center and the injection process is going to start. This situation is better emphasized in fig. 16 by the swirl index distribution in a bowl cross section.

The next figures (17,18,19) show the spray and velocity fields in the piston bowl after the injection start, so highlighting the actual droplet-air interaction within a flow field generated by the gas exchange process. Figure 20 represents the swirl ratio distribution in the combustion chamber calculated at 6° after the injection start. This figure puts into a better evidence that the higher swirl level in the peripheral regions exert a stronger influence on both spray distribution and jet deviation.

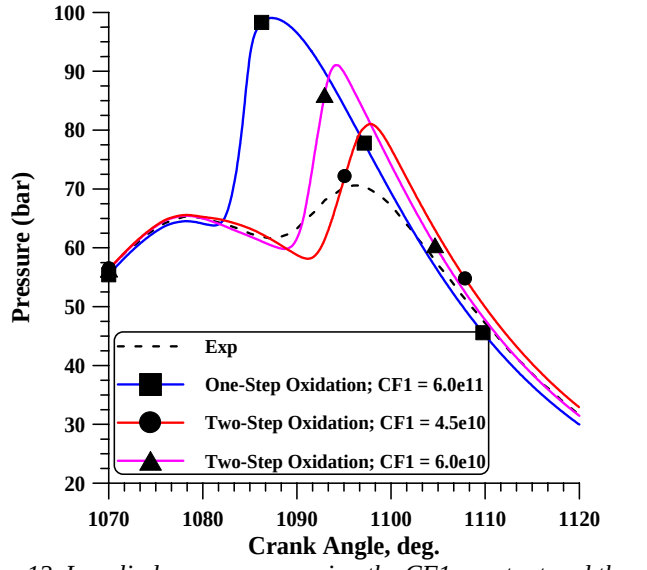

Fig. 12. In-cylinder pressure varying the CF1 constant and the oxidation mechanism. Case EGR =57%

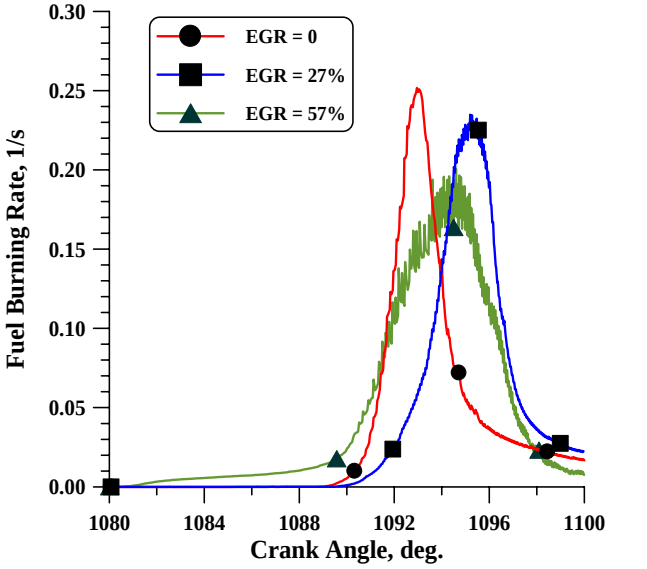

Fig. 13. Fuel burning rates calculated with Wave model

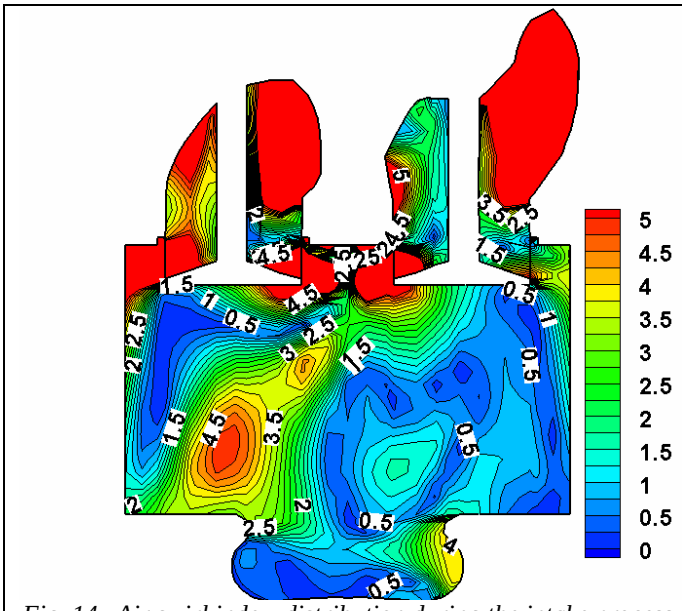

Fig. 14. Air swirl index distribution during the intake process.

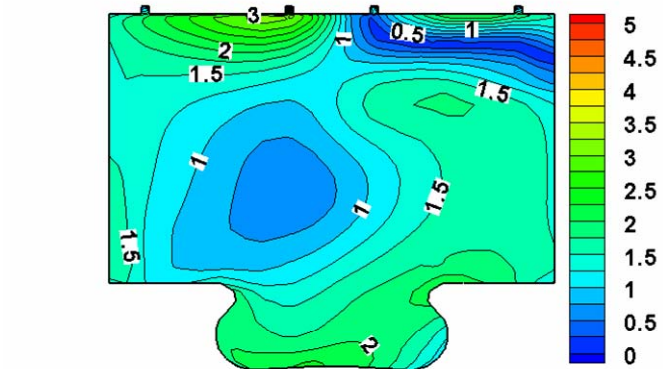

Fig.15. Air swirl index distribution during the compression stroke (80° BTDC)

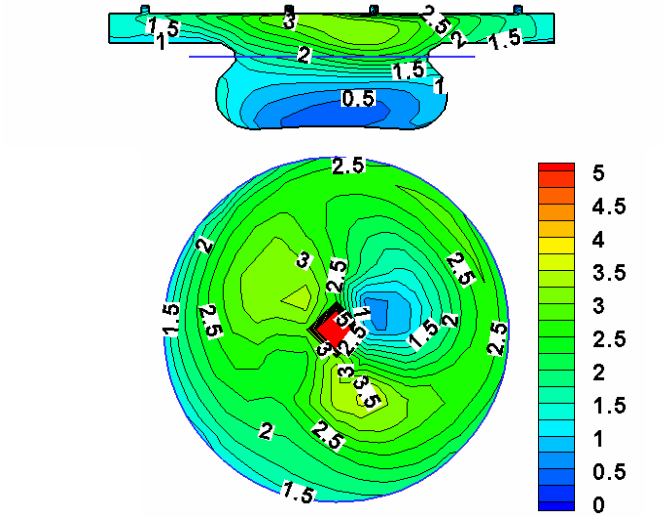

Fig. 16. Air swirl index distribution during the compression stroke (20° BTDC)

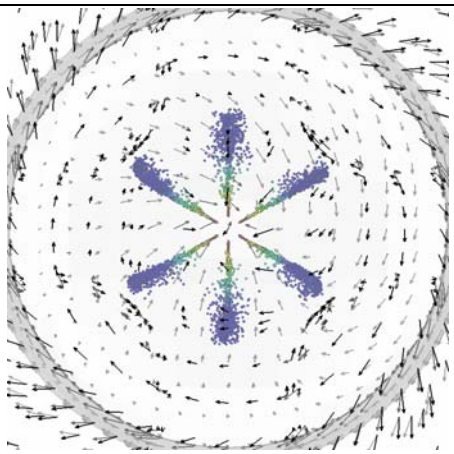

Fig. 17. Spray and velocity field at 4° after injection start

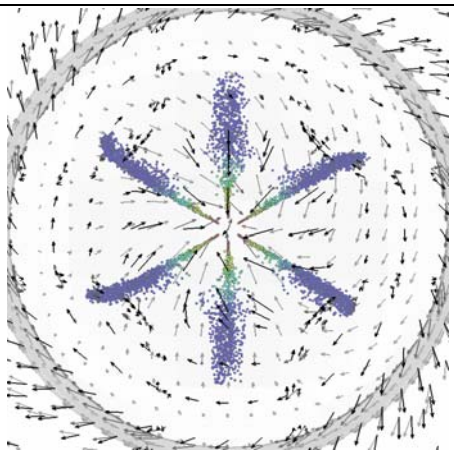

Fig. 18. Spray and velocity field at 6° after injection start

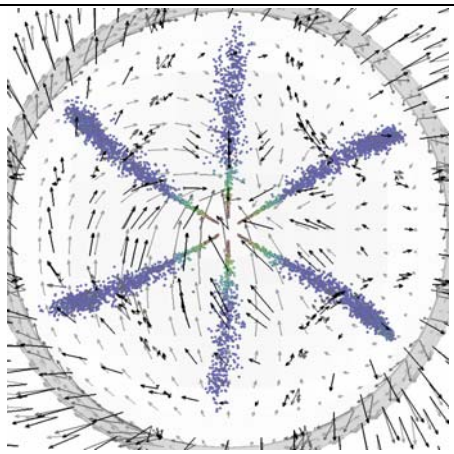

Fig. 19. Spray and velocity field at 9° after injection start

The final CFD and combustion calculations were performed with the KHRT atomization model. In figure 21 the simulation results are shown by varying the B_1 and C_{RT} constants of the model. In particular, the sensitivity to C_{RT} is very low and a value of 0.1 was selected as suggested by Reitz [4]. Besides, in order to reduce the grid cell size sensitivity, as previously discussed, an interpolation method was introduced for estimating the liquid/gas relative velocity as cell-centered values instead of the usual vertex-based values.

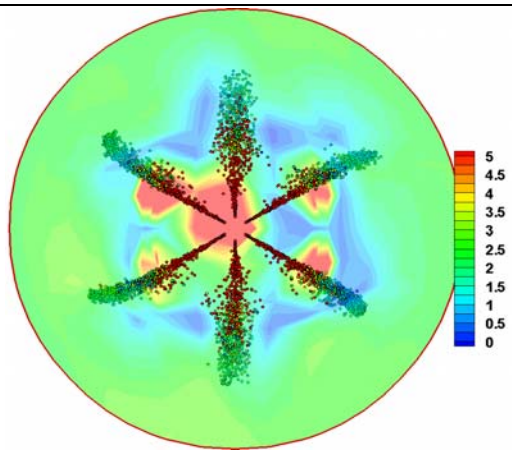

Fig. 20. In-cylinder swirl ratio distribution at 6° after injection start

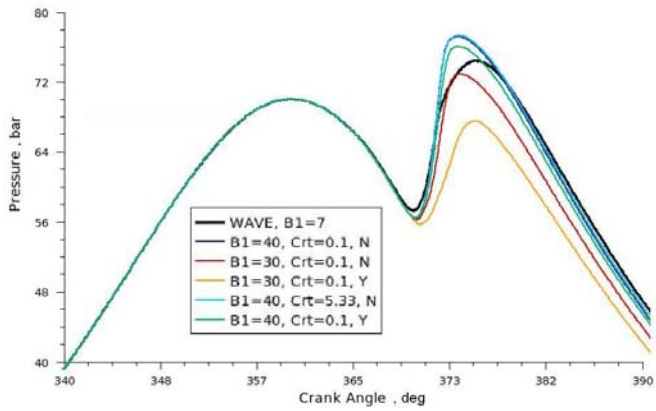

Fig. 21. In-cylinder pressure with Wave and KHRT models. Case EGR =0. 'Y' or 'N' indicates whether or not the liquid/gas velocity interpolation method is activated.

In figure 21, the character 'Y' or 'N' stays for 'with' or 'without' interpolation method. It is possible to observe that the vertex-based method leads to an over-estimation of the pressure levels, so that the interpolation method appears to be more appropriate when dealing with non-well refined meshes.

In order to analyze the sensitivity of the system to the B_1 constant, the effect of a decrease from a value of 40 [4] to 30 was examined. When varying the break-up timing related with B_1, both the liquid penetration and the vapour distribution undergo relevant changes as shown in figures 22 and 23. A lower pressure curve peak is attained in the case B_1=30 as a consequence of the lower jet penetration and of the less uniform fuel distribution.

The last considerations suggested that the B_1 value is worthy of a new expressly addressed optimization and a value of 38 was selected as the best compromise for fitting the experimental data at the different EGR levels. Figures 24 and 25 compare the pressure trends and the fuel burning rate calculated with the two atomization models (*Wave* and *KHRT*) in the case with an EGR rate of 57%. The smoother combustion behaviour that results from the *KHRT* model also allows better results in terms of NO concentration to be expected.

Finally, in the figure 26 and 27 CO and thermal NO concentrations are plotted for the three cases examined with variable EGR rate. Higher *EGR* rates involve a CO increase that partially diminishes the benefits from the relevant decrease in nitric oxide production. It must be underlined that these well established trends are obtained after a reliable estimation of the residual contents after the gas exchange process. Figure 27 also compares the results of the numerical results with the *Wave* and the *KHRT* models. The latter leads, in all cases, to a reduction of the predicted contents in thermal NO, as a result of the smoother combustion development, already observed in figs. 24 and 25. The overall comparison with the emission data from experiments confirms that the latter model would be helpful to a more accurate prediction of the NO_x decrease with the EGR ratio. The qualitative agreement of the nitric oxide trend does not still correspond to a satisfactory fitting of experimental data with the numerical results. Such a consideration clearly confirms that a careful assessment of the combustion models is needed after the flow and atomization model setup.

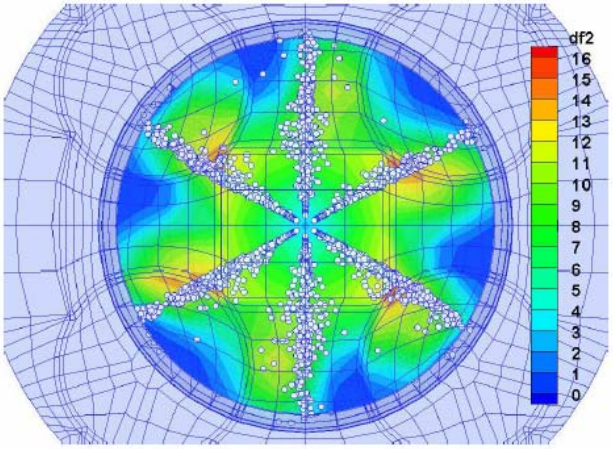

Fig. 22. Spray and fuel vapour distribution in the bowl. KHRT model with B1=40.

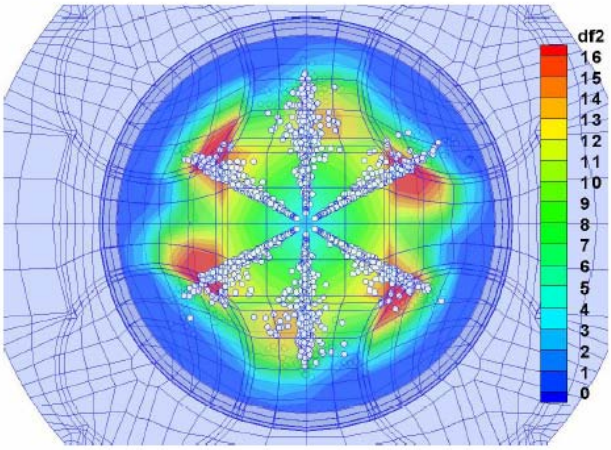

Fig. 23. Spray and fuel vapour distribution in the bowl. KHRT model with B1=30.

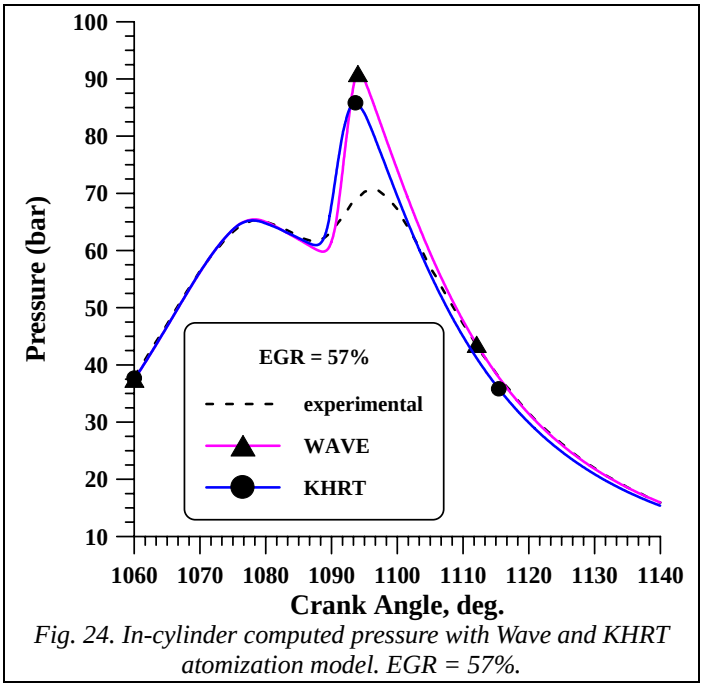

Fig. 24. In-cylinder computed pressure with Wave and KHRT atomization model. EGR = 57%.

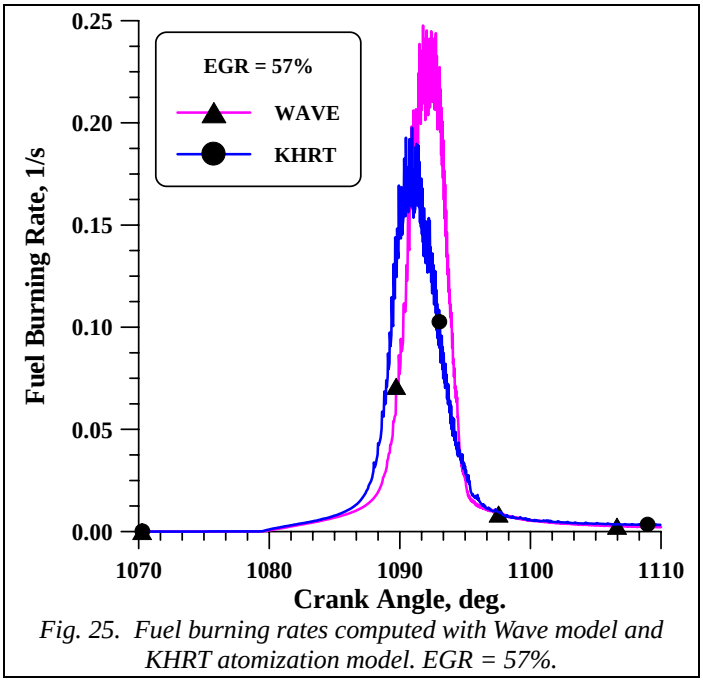

Fig. 25. Fuel burning rates computed with Wave model and KHRT atomization model. EGR = 57%.

CONCLUSIONS

The authors have addressed this paper to a comprehensive assessment of several problems that arise when dealing with the CFD simulation of an up-to-date common-rail diesel engine. Starting from the selection of the most appropriate break-up model for high pressure driven liquid jets, they have proceeded with examples showing both the flow field and the air-spray interaction and, finally, with the comparison of the pressure cycles and combustion developments with the related pollutant formation at different EGR levels.

Some encouraging results have been achieved in terms of optimized selection of the main constant of the break-up sub-

models for a reliable engine simulation in a wide range of EGR levels. Nevertheless, some problems are left open, like those referring to a proper choice of the oxidation mechanisms for a satisfactory description of the combustion development with increased inert contents in the reactants, as resulting from high EGR rates.

The future improvements of both the atomization and combustion sub-models will therefore address the authors' work to give a more appreciable contribution to the theoretical studies and design challenges of the next generation diesel engines.

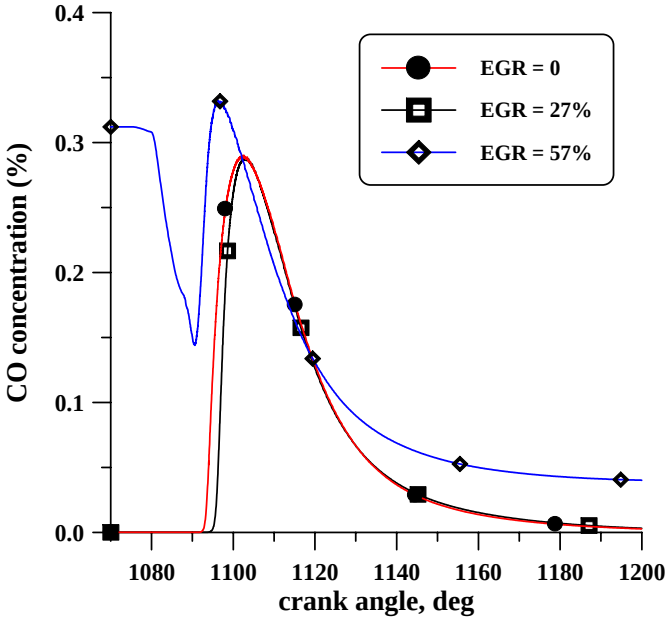

Fig. 26. Calculated CO concentration with variable EGR rate. KHRT atomization model.

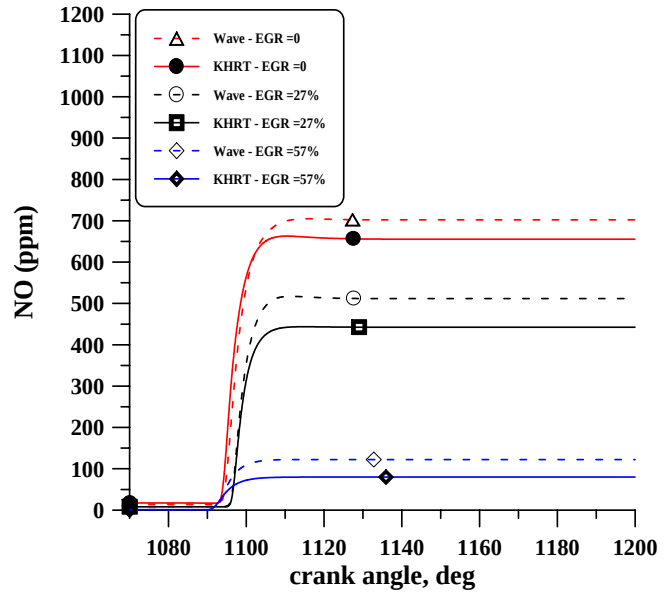

Fig. 27. Calculated NO concentration with variable EGR rate. Wave and KHRT atomization models.

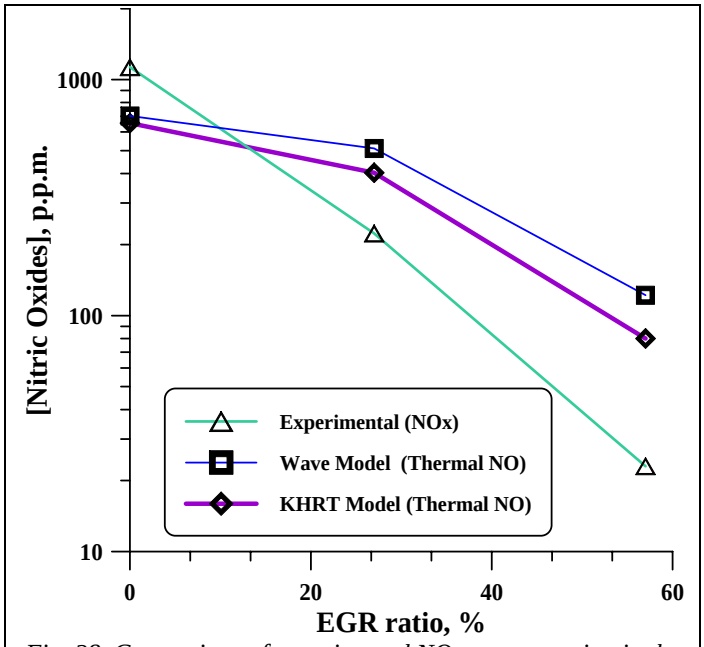

Fig. 28. Comparison of experimental NOx concentration in the exhausts with the numerical results from different atomization models.

ACKNOWLEDGMENTS

The results in this paper have been obtained in the course of cooperation with BOSCH-CVIT/EAR, which is hereby acknowledged for providing engine operating and experimental data.

REFERENCES

[1] O'Rourke P.J.,. Amsden, 1987, A.A, The TAB Method for Numerical Calculation of Spray Droplet Break up, SAE paper 872089.

[2] Reitz R.D., Diwakar R., 1987, Structure of High-Pressure Fuel Sprays, SAE paper 870598.

[3] Reitz R.D, 1987, Modelling Atomisation Processes in High-Pressure Vaporising Sprays, Atomisation and Sprays Tech., vol.3, pp. 309-337.

[4] Beale, C., Reitz R.D., 1999, Modelling Spray Atomization with the Kelvin-Helmholtz/Rayleigh-Taylor hybrid model, Atomization and Sprays, vol.9,pp.623-650.

[5] Amsden A.A., 1997, "KIVA-III v: Block structured KIVA program Engine with vertical or canted valves", LA – Los Angeles 13313 – MS, Los Alamos.

[6] Bozza, F., Cameretti, M.C, Senatore, A.,Tuccillo, R., 1997, "Experimental Investigation and Numerical Modelling of a Advanced Turbocharged d.i. Diesel Engine", SAE paper 970057.

[7] Belardini, P., Bertoli, C., Cameretti, M.C., 1998, "Numerical Analysis on the Influence of Jets Break-up Model Formulation on Diesel Engines Combustion Computations", in ATOMIZATION AND SPRAYS, vol.8, pp123-154, april 1998.

[8] T . F. Su, M. A. Patterson, R. D. Reitz, and P. V. Farrell, 1996, "Experimental and Numerical Studies of High Pressure Multiple Injection Sprays". SAE Paper 960861.

[9] Abrugia, G., Cameretti, M.C., 1998, "Droplet Breakup Modelling of the Evaporating Diesel Fuel Spray by using the FIRE Code", Proc. of ILASS -Europe '98.
[10] Cameretti M.C., Tuccillo R., 2000, “Three-Dimensional Mixture Formation Modeling for Liquid Fuel Spray in a Gas Turbine Combustor”, proc. of 16th. ILASS Europe Conference, pp. IV.3.1 – IV.3.VI, ed. Technical University of Darmstadt.
[11] Patterson, M.A., Kong, S.C, Hampson, G.J, Reitz, R.D.,:1994, "Modelling the Effect of Fuel Injection Characteristics on Diesel Engine Soot and NOx Emissions", SAEpaper 940523.
[12] Liu, A.B., Mather, D., Reitz, R.D., 1993, "Effect of Drop Drag and Break-up on Fuel Sprays", SAE paper 930072.
[13] R. Rotondi, G. Bella, C. Grimaldi, L. Postrioti, 1993, Atomization of High-Pressure Diesel Spray: Experimental Validation of a New Breakup Model. SAE Paper 2001-01-1070, 2001.
[14] K. Huh, A. D. Gosman, 1991, “A Phenomenological Model of Diesel Spray Atomization”, Proceedings of The International Conference on Multiphase Flows, Tsukuba, Japan, 1991.
[15] M.A.Patterson, R.D.Reitz, 1998,. „Modeling the Effects of Fuel Spray Characteristics on Diesel Engine Combustion and Emission” SAE Paper 980131.
[16] Amit Bhave, Markus Kraft, Fabian Mauss, Aaron Oakley and Hua Zhao, 2005, “Evaluating the EGR-AFR Operating Range of a HCCI Engine”, SAE paper 2005-01-0161
[17] Bianchi, G.M., and Pelloni, P., 1999, “Modelling the diesel fuel spray breakup by using a hybrid model”, SAE Paper 1999-01-0226.
[18] Cameretti M.C., Reale F, and Tuccillo R., 2006, “Cycle Optimization and Combustion Analysis in A Low-NOx Micro-Gas Turbine”, ASME Paper GT2006-90240.
[19] Cameretti M.C., Reale F, and Tuccillo R. , 2007,”NOx Suppression from a Micro-Gas Turbine Approaching the Mild-Combustion Regime, ASME Paper GT2007-27091.
[20] Babajimopoulos, A., Assanis, D.N., and Fiveland, S.B., 2002, “An Approach for Modeling the Effects of Gas Exchange Processes on HCCI Combustion and Its Application in Evaluating Variable Valve Timing Control Strategies, SAE paper 2002-01-2829
[21] Assanis, D.N., and Fiveland, S.B., 2002, “Development and Validation of a Quasi-Dimensional Model For HCCI Engine Performance and Emissions Studies Under Turbocharged Conditions”, SAE paper 2002-01-1757
[22] Babajimopoulos, A., Lavoie, G.A., and Assanis, D.N., 2003, “Modeling HCCI Combustion with High Levels of Residual Gas Fraction – A Comparison of Two VVA Strategies”, SAE paper 2003-01-3220.
[23] Jacobs, T.J., et al., 2005, “ Lean and Rich Premixed Compression Ignition Combustion in a Light-Duty Diesel Engine”, SAE paper 2005-01-0166
[24] Chryssakis. C.A., and, Assanis, D.N., 2005, “A Secondary Atomization Model for Liquid Droplet Deformation and Breakup under High Weber Number Conditions”, proc. Of 18th ILASS America
[25] Amit Bhave, et al., 2005, “Evaluating the EGR-AFR Operating Range of a HCCI Engine”, SAE 2005-01-0161.
[26] Magnussen, B.F. and Hjertager, B.H., 1977, “On Mathematical Modeling of Turbulent Combustion with Special Emphasis on Soot Formation,” 16th. Symposium on Combustion, The Combustion Institute, Pittsburgh.
[27] Stringer, F.W., Clarke A., E., and Clarke, J.S., 1970, "The Spontaneous Ignition of Hydrocarbon Fuels in a Flowing System," proc. Instn Mech. Engrs, vol. 184, pt. 3J, 1969-1970.
[28] Zel’dovich, Y.B., Sadovnikov, P.Y., Frank-Kamenetskik, D.A., 1947, "Oxidation of Nitrogen in Combustion," Academy of Science of SR, Institute of Chemical Physics, Moscow-Leningrad.